BACHELOR

Observer Design and System Identification of the E-puck Setup

van der Horst, Anne

Award date:
2020

EINDHOVEN UNIVERSITY OF TECHNOLOGY

Department of Mechanical Engineering
Dynamics and Control

Observer Design and System Identification of the E-puck Setup

4WC09 Bachelor Final Project
Second semester 2019/2020
DC 2020.081

A. van der Horst 1267876

ir. W.J. Scholte Project coordinator
dr. ir. T.P.J. van der Sande Project coordinator

Eindhoven
June 29, 2020

Abstract - *In this project, two observers are developed for the e-puck setup present at the Dynamics and Control Department at the Eindhoven University of Technology. The e-puck setup consists of multiple e-puck robots that drive around in a predefined area, where the robots are of an unicycle mobile type. Since there is an angular offset present between the actual and measured pose (position and angle), the robots deviate from their predetermined trajectory. The observers are used to estimate the true pose. They are constructed based on a kinematic model that describes the pose (position and angle) over time for the given inputs velocity $v(t)$ and angular velocity $\omega(t)$. Looking at the kinematic model, two observers similar to an extended Luenberger observer are developed. The first observer is based solely on the outputs of the system. As there is an assumed error on the measurement caused by the angular offset, this error is unknown to the observer. Therefore, the second observer includes an additional state which comprises a constant offset as an additional state. For both observers, the stability and observability have been evaluated to ensure proper functioning. Lastly, the performance of the observers is experimentally determined using multiple tests. The main results are that both observers perform desirably, as the observers function within the requirements for angular offsets of* 0.1 *rad and lower. However, the observer which includes the constant offset is often unstable for different input signals. This observer must thus be treated with care when used in a real life setup.*

List of Symbols

Symbol	Quantity	Unit abbreviation
A	State matrix	-
B	input matrix	-
C	output matrix	-
D	Feedforward matrix	-
E	Error matrix	-
e	Error vector	*Dependent of subscript*
eig	Eigenvalues	*Dependent of matrix*
IC	Initial condition	*Dependent of subscript*
K	Gain matrix	-
r	Radius	m
t	Time	s
t_0	Settling time	s
O	Observability matrix	-
v	Input velocity	m s^{-1}
w	Noise	*Dependent of subscript*
x	Position in the x-direction	m
y	Position in the y-direction	m
y	Output vector	-
z	State vector	-
θ	Rotation	rad
ω	Angular input velocity	rad s^{-1}

Characters	Quantity
$\dot{c}$	Derivative of a variable with respect to time
$\hat{c}$	Observer variable
c_{grad}	Gradient of
c_{GT}	Of the ground truth signal
$c_{measured}$	Of the measured data
c_{model}	Of the model data
$c_{observer}$	Of the observer data
c_{off}	The offset of
c_{offset}	Of the offset observer
c_{output}	Of the output observer
$c_{reduced}$	Reduced version of
c_{true}	Actual version of
c_x	In x-direction
c_y	In y-direction
c_θ	In θ-direction

Contents

Chapter 1

Introduction

The e-puck setup at the Dynamics and Control Department of the Eindhoven University of Technology consists of a confined area in which e-puck robots can drive around. The pose (position and angle) of the robots in the setup is determined using a camera that is mounted above the setup. However, an angular offset between the pose registered by the camera and the actual pose of the e-puck robots has been found. Therefore, the focus of this project is to create an observer to estimate the pose of the e-puck and said angular offset.

1.1 The e-puck setup

The e-puck setup is a setup consisting of multiple mobile robots. These robots have been developed at the Ecole Polytechnique Fédérale de Lausanne, Switzerland, as a collaboration between the Swarm-Intelligent Systems group, the Autonomous Systems Lab and the Laboratory of Intelligent System, their main goal being to develop a miniature robot for educational purposes at university level. To achieve this goal, an easy mechanical structure, good robustness, large potential in its sensors to ensure the robots flexibility, low costs and, of course, user friendliness have been the key features during development. This resulted in a unicycle type robot consisting of two wheels which are driven by miniature stepper motors, equipped with sounds sensors, a 3D accelerometer, proximity sensors and a camera. It also contains a Bluetooth chip that is used to communicate with the e-puck. The project is based on an open hardware concept, allowing everyone to use and develop for it [1]. E-puck robots are used extensively in different types of research; from the dynamical control of a robotic swarm [2] to learning algorithms for small mobile robots [3]. Whilst at the Eindhoven University of Technology, the e-puck setup is used mostly in research related to self-driving cars, it was originally composed to investigate the coordination control of unicycle mobile robots using a virtual structure approach [4].

The setup at the Dynamics and Control Department consists of a white vinyl floor of 3.5 m by 2.5 m which depicts the driving area of the robots, see Figure 1.1.1. The pose of the robots is calculated by processing images from a top mounted camera that detects the markers fitted to the robots, as can be seen in Figure 1.1.2. Through the Bluetooth connection, the e-puck robots are controlled by a MATLAB code that sends the robots a pre-determined trajectory by introducing different angular velocities to the left and right wheel of the robot.

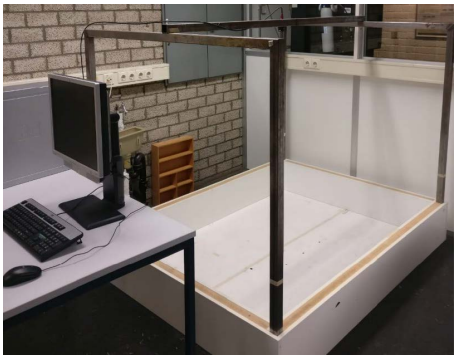

Figure 1.1.1: The e-puck setup at the Dynamics and Control Department

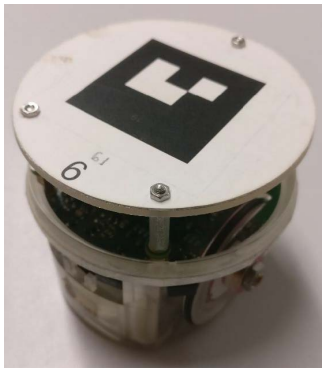

Figure 1.1.2: An e-puck robot as used by the Eindhoven University of Technology

1.2 Project goal and research questions

The pose of the unicycle type robots in the e-puck setup is measured using markers on the robots, which are located by a camera that observes the setup from above. However, an angular offset between the pose of the robots and the expected pose based on the measurements of the camera has been found. This results in the robots deviating from their predetermined trajectory.

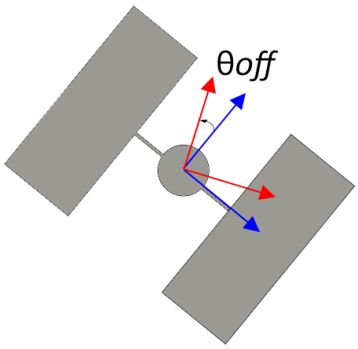

Figure 1.2.1: Schematic top view of an e-puck robot. The blue arrows indicates the actual vehicle frame of the e-puck. The red arrows indicates the vehicle frame of the e-puck robot based on the measurement of the pose by the camera. The angular offset between the two frames and thus also the two poses is given by θ_{off}.

Therefore, the goal of this project is to correct for this offset by creating an observer that estimates the pose of the unicycle.
Following from the project goal, the main research objective is *to develop a state observer for the e-puck robots that estimates the angular offset by use of a kinematic model of the system.* Next to the main research objective, several subquestions are taken into account during the scope of the project, such as:

- How is the model of the e-puck robot best defined?
- What type of observer is required based on the identification of the system?
- How can the unknown angular offset best be estimated and implemented in the design of the observer?

1.3 COVID-19

Due to the outbreak of the COVID-19 virus and the subsequent closure of the Dynamics and Control Department at the university campus, none of the results of this project could be tested on the physical e-puck setup. All results have therefore been verified using either already existing e-puck measurements, or simulated signals generated by MATLAB. The signals are considered to be closely related to the actual setup and therefore representative enough to verify the results of this project. It is thus assumed that the results are reliable and similar results would be obtained if the project was to be verified using the physical setup.

1.4 Thesis outline

Firstly, a short overview of existing linear and non-linear observers is given in Chapter 2 to provide insight in the previously conducted research on this topic. Next, in Chapter 3, the kinematic model of the unicycle system is constructed. Now, an observer can be chosen and its construction is started in Chapter 4. In Chapter 5, an experiment plan is presented and corresponding results are evaluated. Finally, the project is concluded with a conclusion and recommendations are given for future research.

Chapter 2

Related Literature

For many applications in control theory, it is essential to know the state of a system. However, often this state cannot be directly measured. A state observer can estimate the state of a system based on measurements of the input, output and the estimated output provided by the dynamical or kinematic model.
The first to address the designing of observers for linear control systems was D.G. Luenberger. In [5], Luenberger shows that "the design of an observer for a system with M outputs can be reduced to the design of m separate observers for single-output subsystems". Here, m is the number of independent outputs of a state vector of an n^{th} order system. This results in an observer of the form of

$$\dot{\hat{x}} = A\hat{x} + L[y - \hat{y}] + Bu \tag{2.0.1}$$

for the state of a linear time-invariant (LTI) system

$$\begin{aligned} \dot{x} &= Ax + Bu \\ y &= Cx + Du \end{aligned} \tag{2.0.2}$$

However, as the dynamics of e-puck unicycle system are most likely not linear, an observer is required that would be able to function on a nonlinear system as well. This can be done by adapting existing observers for linear systems, as is shown by M. Zeitz [6]. In this paper, the Luenberger observer is extended for nonlinear systems. Here, the observer for the single-output systems

$$\begin{aligned} \dot{x} &= f(x, u) \\ y &= h(x, u) \end{aligned} \tag{2.0.3}$$

is proposed to be of the form of

$$\dot{\hat{x}} = f(\hat{x}, u) + g(\hat{x}, u^*)[y - h(\hat{x}, u)] \tag{2.0.4}$$

where u^* contains the derivatives of u and where $g(\hat{x}, u^*)$ is a function that depends on the estimated states of the system. This gain factor is later determined using canonical coordinates.
A similar option is discussed in a paper on state observers for nonlinear systems [7]. K.

Busawon and M. Saif discuss that constant gain observers can be designed for nonlinear systems. In contrast to the observer of M. Zeitz, this observer also makes use of an observability matrix $M(\xi, t)$ and a diagonal matrix Δ_θ that is dependent on an introduced variable θ.

$$\dot{\hat{x}} = f(\hat{x}, t) + M^{-1}(\hat{x}, t)\Delta_\theta^{-1}K(y - h(\hat{x}, t)) \tag{2.0.5}$$

Also, the importance of matrix $M(\xi, t)$ being full rank and matrix A-KC being Hurwitz is discussed, since both must be obtained for the observer to be operational. Here, matrices A and C are $n \times n$ and $1 \times n$ constant matrices of the Brunowsky form, and K is the gain matrix. A few hands-on examples of this type of observers on nonlinear systems is given by [8]. V. Sundarapandian shows the observer of the form of

$$\dot{\hat{x}} = f(\hat{x}) + K[y - h(\hat{x})] \tag{2.0.6}$$

to function properly on different kinds of nonlinear systems, of which most are different types of pendulum systems.

Apart from extended linear observers, also nonlinear observers exist that can be applied on nonlinear systems. However, nonlinear observer design requires a different approach. The first observer design for nonlinear systems was proposed by F.E. Thau [9], after which the attention for observers for nonlinear control systems grew in control systems literature.
One of the main focus areas of nonlinear observer design, is the design of observers for systems that can be linearized using a linearizing transformation, often denoted by $z = \Phi(x)$. As suggested by A.J. Krener and A. Isidori in [10], a nonlinear system

$$\begin{aligned} \dot{\xi} &= f(\xi) \\ y &= h(\xi) \end{aligned} \tag{2.0.7}$$

is observed to be the result of applying a nonlinear output injection to a linear system of the form of $\dot{x} = Ax, y = Cx$. This results in the system

$$\begin{aligned} \dot{x} &= Ax + \varphi(y) \\ y &= Cx \end{aligned} \tag{2.0.8}$$

followed by the nonlinear change of coordinates $\xi = \xi(x)$. If this is the case and $\varphi(y)$ and $\xi(x)$ can be found, the observer for the nonlinear system can be constructed almost as easily as for the linear case.

Another form of nonlinear observers is the sliding-mode observer. Sliding-mode observers are both applicable for linear and nonlinear systems. Its use is justified by the peaking phenomenon that is sometimes present in Luenberger observers. This is caused by high observer gains, making the observer impractical or even unsafe to use. A sliding-mode observer is used in such a case to bring the estimated state's error to zero, even if a measurement error should be present. As discussed by S.K. Spurgeon [11], for a non-linear system

$$x^{(n)} = f(x, t) \tag{2.0.9}$$

where $f(x,t)$ is defined as the non-linear function of the system state, the sliding mode observer is defined as follows

$$\begin{aligned}\dot{\hat{x}}_1 &= -\alpha_1 e_1 + \hat{x}_2 - k_1 sgn(e_1)\\ \dot{\hat{x}}_2 &= -\alpha_2 e_1 + \hat{x}_3 - k_2 sgn(e_1)\\ &\ldots\ldots\\ \dot{\hat{x}}_n &= -\alpha_n e_1 + \hat{f} - k_n sgn(e_1)\end{aligned} \tag{2.0.10}$$

where $e_1 = \hat{x}_1 - x_1$ and where $\hat{f}$ is an estimate of $f(x,t)$. For x_1, the single measurement available is used. Here, the constants a_{i} are usually chosen as one would for a Luenberger observer to establish asymptotic error decay.

Sliding-mode observers, however, have been found to be inferior in dealing with dynamic uncertainties, disturbances and sensor noise compared to extended state observers (ESO) [12]. For the first time introduced by J. Han in 1995 [13], the nonlinear ESO is a rather unique observer design. The observer is independent of mathematical models of plants, on the contrary to observers such as the Kalman Filter and the Luenberger observer, thus achieving innate robustness. As proposed by Han for an n-dimensional single-input single-output (SISO) nonlinear system

$$\begin{aligned}x^{(n)}(t) &= f(t, x(t), \dot{x}(t), ..., x^{(n-1)}(t)) + w(t) + u(t)\\ y(t) &= x(t)\end{aligned} \tag{2.0.11}$$

where u is the input, y the output, f a possibly unknown function of the system and w the unknown disturbance, the following ESO exists:

$$\begin{aligned}\dot{\hat{x}}_1(t) &= \hat{x}_2 - \alpha_1 g_1(\hat{x}_1(t) - y(t))\\ \dot{\hat{x}}_2(t) &= \hat{x}_3 - \alpha_2 g_2(\hat{x}_1(t) - y(t))\\ &\ldots\ldots\\ \dot{\hat{x}}_n(t) &= \hat{x}_{n+1} - \alpha_n g_n(\hat{x}_1(t) - y(t)) + u(t)\\ \dot{\hat{x}}_{n+1}(t) &= -\alpha_{n+1} g_{n+1}(\hat{x}_1(t) - y(t))\end{aligned} \tag{2.0.12}$$

The main idea of the ESO is that the state $\hat{x}_i$ can be considered to be an approximation of the state x_i and the disturbance $f + w$. This is done by choosing the functions g_i and through regulating a_i. Many studies have shown that by choosing nonlinear functions for g_i and parameters for a_i, the observer has a satisfactory robustness and adaptability.
However, the choice of functions g_i must essentially be made experimentally. Therefore, to apply this conveniently in practice, Z. Gao [14] proposes to use instead a linear extended state observer (LESO).

All in all, many different types of observers have been designed over time to fit linear and nonlinear control systems, each with their own set of benefits and disadvantages. All types of observers are model dependent, as becomes apparent by comparing, for example, the models

described in (2.0.1), (2.0.8) and (2.0.11). Because of this, it is important to first derive the correct kinematic model of the system before choosing a fitting observer. As the model for the e-puck is yet to be determined, the decision for which observer to work with for this project is postponed until after the kinematic model is constructed and verified.

Chapter 3

E-puck model

Kinematic models are generally used to describe the behaviour of an object over time. In the case of the unicycle, it is an important tool in predicting the pose of the unicycle. It is used to obtain a first impression of the offset of the e-puck unicycle, and it provides a foundation upon which the observer is later built. This chapter includes the principles behind the kinematic model in Section 3.1. The model output and the results and verification of the model are discussed in Sections 3.2 and 3.3 respectively. Also, an error analysis is conducted in Section 3.4 to verify that remaining differences between the model output and the measured e-puck output are not caused by model flaws.

3.1 Model assumptions

The e-puck robot is a unicycle type robot, and moves with a velocity $v(t)$ and an angular velocity $\omega(t)$. These states are thus considered to be the input functions of the kinematic model. The pose of the unicycle, indicated by the states $x(t)$, $y(t)$ and $\theta(t)$, is defined as the output. The definitions of these states are visualized in Figure 3.1.1. The output functions are expressed in absolute coordinates, with respect to a set axis fixed in the real world. In this case, the origin of this axis is located in the lower left corner of the e-puck setup, as evaluated by the overhead camera. Since the input functions also refer to the same origin, no further transformations between the input and the output are required.

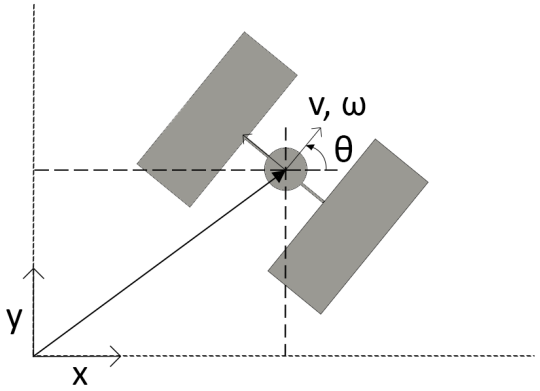

Figure 3.1.1: Variable definitions unicycle model

Using the definitions of Figure 3.1.1, $\dot{x}$ and $\dot{y}$ are equal to the x- and y-components of the velocity of the unicycle respectively and $\dot{\theta}$ is equal to the angular velocity.

3.1.1 Kinematic constraints

A kinematic model is deemed valid if the system has zero degrees of freedom, as is shown in [15]. For this to be true, the number of coordinates must be equal to the number of constraints. For the unicycle case, one holonomic and two non-holonomic constraints can be identified:

- The rotational velocity is equal to the input state $\omega(t)$, with a maximum of $\omega(t) = 5$ $rad\, s^{-1}$
- The forward velocity is equal to $v(t)$, with a maximum of $v_{max} = 0.13\ m\, s^{-1}$
- The lateral velocity in the vehicle frame is zero, in other words, no wheel side slip occurs: $-\dot{x}\sin\theta + \dot{y}\cos\theta = 0$

Since the number of constraints is equal to the number of coordinates, the assumption for a kinematic system is valid.

3.1.2 Kinematic input-output relation

The relation between the output states and the input states can now be derived and expressed as

$$\dot{z} = \begin{bmatrix} \dot{x} \\ \dot{y} \\ \dot{\theta} \end{bmatrix} = \begin{bmatrix} v\cos\theta \\ v\sin\theta \\ \omega \end{bmatrix} \tag{3.1.1}$$

To acquire the output $z = \begin{bmatrix} x & y & \theta \end{bmatrix}^T$, the given functions must then be integrated over time.

3.2 Model output

In order to see if the model shows reliable output data, simple functions for v and ω, of which the expected outputs are known prior to the calculations of the model, are entered as input functions. This way, errors in the model can be detected early on so that, when actual measurement data from the setup is used, any distinguishable offsets are known not to be caused by a model error.

Starting of simply, a linear velocity profile and an angular velocity equal to 0 are assigned as input. This should result in an output where the unicycle drives in a straight line along the x-axis, since θ equals 0. In Figure 3.2.1, the trajectory calculated by the model of the unicycle is shown. As expected, a straight line is seen along the x-axis. At $t = 1$, the unicycle stops at $x = 0.065$. This is exactly the value of the velocity integrated over time, and therefore the results are correct.

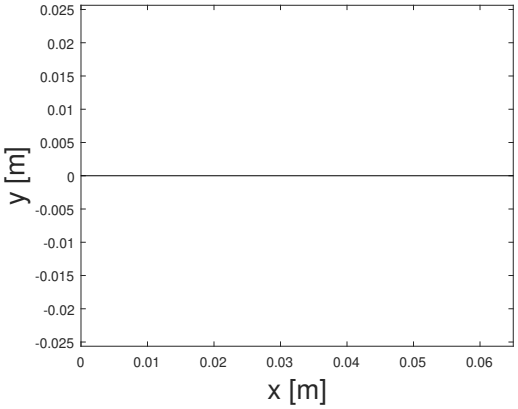

Figure 3.2.1: The trajectory of the unicycle in the xy-plane for $v = v_{\max} t \ m\ s^{-1}$ and $\omega = 0$ $rad\, s^{-1}$, initial conditions set as $z = \begin{bmatrix} 0 & 0 & 0 \end{bmatrix}^T$

Next, a different trajectory is set for the unicycle. Still, a constant acceleration is used, but now a value of $4\pi t \ rad\, s^{-1}$ is assigned to ω. A trajectory that follows the shape of a circle is expected, with a radius of $0.01\ m$, as calculated using $r = v/\omega$. This corresponds with the result in Figure 3.2.2, which shows that the function of ω is correctly implemented. To see if the output behaves accordingly for a changed function of v, the velocity is halved. This should result in a trajectory of a circle with the radius half of the previous result, namely $0.005\ m$. Figure 3.2.3 shows the expected result, and therefore shows that the function of v is correctly implemented as well.

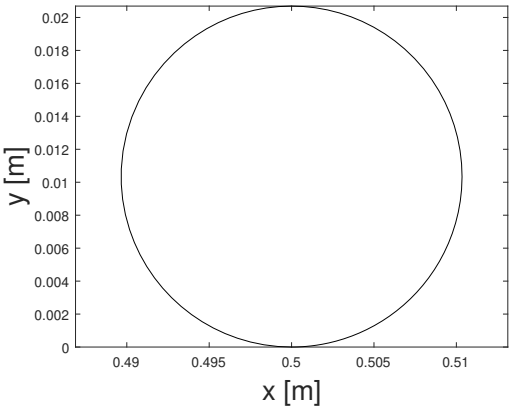

Figure 3.2.2: The trajectory of the unicycle in the xy-plane for $v = v_{\max} t \ m\ s^{-1}$ and $\omega = 4\pi t \ rad\ s^{-1}$, initial conditions set as $z = \begin{bmatrix} 0.5 & 0 & 0 \end{bmatrix}^T$

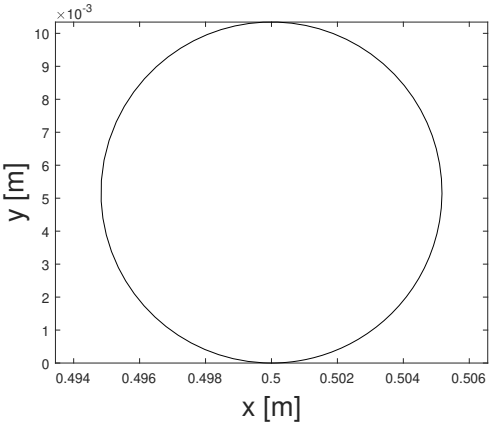

Figure 3.2.3: The trajectory of the unicycle in the xy-plane for $v = 0.5 v_{\max} t \ m\ s^{-1}$ and $\omega = 4\pi t \ rad\, s^{-1}$, initial conditions set as $z = \begin{bmatrix} 0.5 & 0 & 0 \end{bmatrix}^T$

3.3 Results and verification

In order to see if the derived kinematic model is an accurate representation of the reality, the output functions of the kinematic model must be compared to the output functions of the

physical setup. This is done by measuring the output of the e-puck robot based on a certain input. The same input is then used in the kinematic model, after which the different outputs can be compared. However, due to the closing of the university concerning the COVID-19 virus, no test data could be obtained. Therefore, previously acquired test data from the project coordinator is used instead.

The data acquired during testing is stored in so called hist cells or hist vectors, hist being short for history. This data contains all the information of the unicycle during real time testing, such as the input states v and ω and the output states x, y and θ. Next to that, a time vector and the gradient of the time vector are saved. Now, the input states and the time vector of the measurement data are used as input functions of the kinematic model.

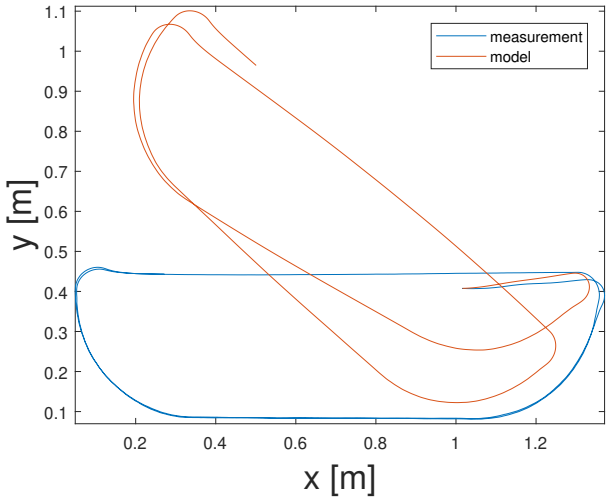

Figure 3.3.1: The measurement output data showing the trajectory of the unicycle in the xy-plane during testing, and the model output data showing the predicted trajectory of the unicycle based on the input functions of the measurement data, also in the xy-plane.

In Figure 3.3.1, the trajectory of the unicycle during testing is shown, as the trajectory of the unicycle as predicted by the model. Ideally, both outputs would be exactly the same.
Even though the general pathway in both figures is distinctively the same, deviations between the paths can be seen. This is most likely due to the before described angular offset and possible noise from the test setup, as can be described by:

$$x_{measured} = x_{true} + x_{off} + w_x \tag{3.3.1}$$

The measurement data consists of a sum of multiple variables for the measurement of the output state x. Firstly, the data includes the actual output data of the unicycles location, x_{true}. This variable also includes measurement deviations, such as for example, deviations caused by friction of the wheels of the e-puck. Secondly, it includes an offset x_{off}. This offset comprises the deviations caused by the before described angular offset. Lastly, a certain noise w_x is present, consisting of noise of the test setup, for example noise from the position measurement. Both the offset and the noise contribute to the seen deviations in Figure 3.3.1.

3.4 Error analysis

In order to obtain better insight in the differences between the measurement data and the data obtained from the kinematic model, an error analysis is performed. This is done by subtracting the measurement data from the model data. However, by doing so, the error is most likely to build up over time. To remove this influence of previous errors on the error at a certain time t, the so called gradient is determined, as is shown in (3.4.1) for the state x.

$$e_{grad,x} = \nabla(x_{model} - x_{measured}) \tag{3.4.1}$$

The results of the analysis can be seen in Figures 3.4.2, 3.4.4 and 3.4.6. When comparing the gradient of the error of the state x to the model and measurement data in Figure 3.4.1, the error equals 0 at the same point in time as the graph of the model output and the measured output intersect, as expected. Furthermore, the output state x seems to have the largest errors around the peaks in Figure 3.4.1. When comparing this figure to Figure 3.3.1, the peaks correspond with the maximum and minimum values for the state. Because of the angular offset between the two results, the values for the maximum and minimum are lower for the output of the kinematic model. The same behavior can be seen in Figure 3.4.3, however here the maximum values for the kinematic model output are significantly larger than the measured output. This difference can again be attributed to the angular offset in Figure 3.3.1, where the state y of the model output data is seen to differ over a larger range.
The gradient of the error of the state θ is relatively small and constant, which can be seen in Figure 3.4.6. However, when taking a closer look at Figure 3.4.5, the angular offset becomes apparent. Almost over the complete trajectory of the unicycle, the measurement data displays a larger value for state θ than the model data.

In short, the error analysis of all three output states points towards the fact that the deviations are caused by an angular offset, and that the kinematic model of the unicycle is a reliable representation of the unicycles behavior.

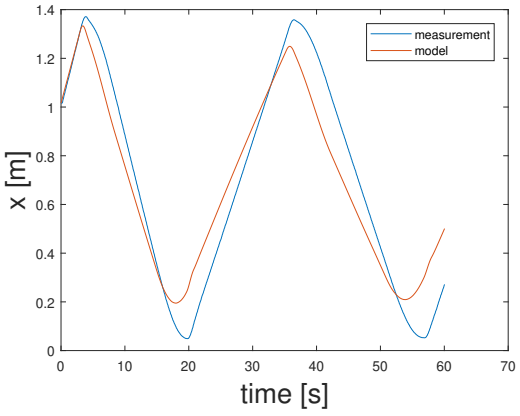

Figure 3.4.1: The output state x of the measurement data and of the model with respect to time

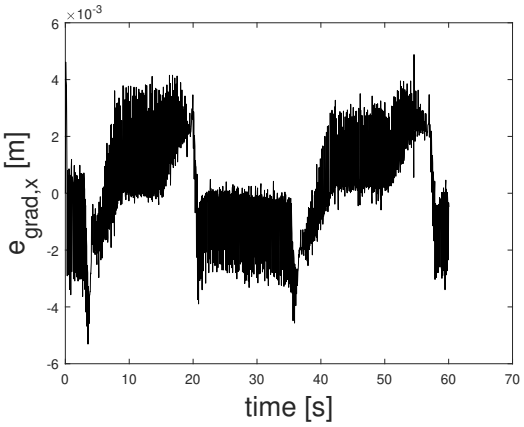

Figure 3.4.2: The gradient of the error of the output state x with respect to time

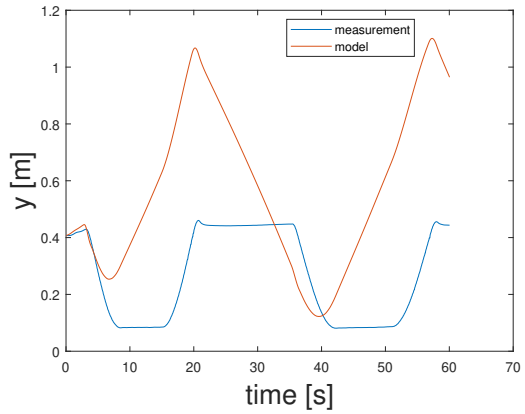

Figure 3.4.3: The output state y of the measurement data and of the model with respect to time

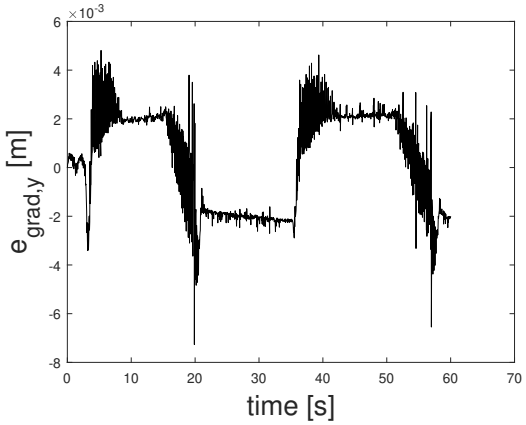

Figure 3.4.4: The gradient of the error of the output state y with respect to time

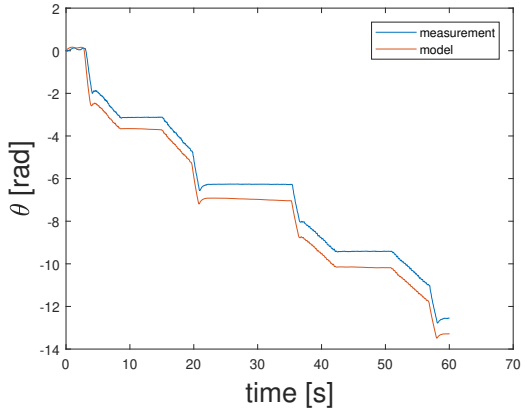

Figure 3.4.5: The output state θ of the measurement data and of the model with respect to time

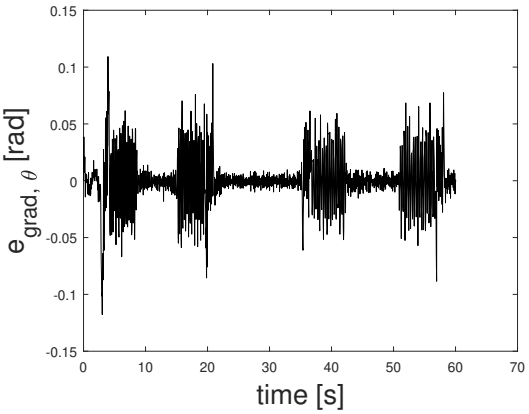

Figure 3.4.6: The gradient of the error of the output state θ with respect to time

Chapter 4

The state observer

This chapter includes two different kinds of observers. One that is solely based on the system outputs, the so-called output observer in Section 4.1, and one that is based on the system outputs and an additional state that estimates the angular offset, the so-called offset observer in Section 4.2. For both observers, the basic principles of their construction are provided, as well as their requirements in terms of observability and stability.

4.1 Output observer

In order to create an observer, first the state space representation of the system must be identified. Since the system inputs are defined as v and ω and the system outputs are chosen to be x, y and θ, the nonlinear system can be defined as:

$$\begin{aligned} \dot{z} = f(y,u,t) &= \begin{bmatrix} cos(\theta) & 0 \\ sin(\theta) & 0 \\ 0 & 1 \end{bmatrix} \begin{bmatrix} v \\ \omega \end{bmatrix} \\ y = h(z,t) &= \begin{bmatrix} 1 & 0 & 0 \\ 0 & 1 & 0 \\ 0 & 0 & 1 \end{bmatrix} \begin{bmatrix} z_1 \\ z_2 \\ z_3 \end{bmatrix} \end{aligned} \tag{4.1.1}$$

Where the state vector z is defined as $\begin{bmatrix} x & y & \theta \end{bmatrix}^{\mathrm{T}}$ and $\dot{z}$ as $\begin{bmatrix} \dot{x} & \dot{y} & \dot{\theta} \end{bmatrix}^{\mathrm{T}}$. Here, the chosen output y is thus equal to z. As all output vectors and state vectors are time dependent, this is not further indicated in equations to improve readability.

First it must be checked if the system in its current definition is observable, according to [8]. In order to check this, the nonlinear system of (4.1.1) needs to be linearized to a system of the form of:

$$\begin{aligned} \dot{x} &= Ax + Bu \\ y &= Cx + Du \end{aligned} \tag{4.1.2}$$

This can be done by re-writing (4.1.1) in the following form

$$\dot{z} = f(z) + g(z)u \tag{4.1.3}$$

where, when $\mathbf{g}(z,u)$ is assumed to be equal to $g(z)u$, the Jacobian is used to linearize the system about the unicycle's trajectory. For the state matrix A, the Jacobian of the linearized system, subjected to an equilibrium or trajectory, is given by

$$J := D\mathbf{g}(z,u) = \frac{\partial \mathbf{g}(z,u)}{\partial z} = \begin{bmatrix} 0 & 0 & -v\sin\theta \\ 0 & 0 & v\cos\theta \\ 0 & 0 & 0 \end{bmatrix} \tag{4.1.4}$$

From this it follows that the new state space representation becomes

$$\begin{aligned} \dot{z} &= \begin{bmatrix} 0 & 0 & -v\sin\theta \\ 0 & 0 & v\cos\theta \\ 0 & 0 & 0 \end{bmatrix} \begin{bmatrix} x \\ y \\ \theta \end{bmatrix} + \begin{bmatrix} cos(\theta) & 0 \\ sin(\theta) & 0 \\ 0 & 1 \end{bmatrix} \begin{bmatrix} v \\ \omega \end{bmatrix} \\ y &= \begin{bmatrix} 1 & 0 & 0 \\ 0 & 1 & 0 \\ 0 & 0 & 1 \end{bmatrix} \begin{bmatrix} x \\ y \\ \theta \end{bmatrix} \end{aligned} \tag{4.1.5}$$

Using (4.1.5), the observability matrix can be determined, as seen in (4.1.6). For the observability matrix, n is equal to the number of state variables, being 3 in this case. Now, the system is deemed observable if the rank of the observability matrix $O(C,A)$ is equal to n. When looking at the O-matrix of the e-puck system, it becomes apparent that the system is always observable. This is due to the fact that the matrix C already has a full rank, thus satisfying the requirement of observability already, regardless of the matrices CA until CA^{n-1}.

$$O(C,A) = \begin{bmatrix} C \\ CA \\ \cdot \\ \cdot \\ CA^{n-1} \end{bmatrix} \tag{4.1.6}$$

Now, for the system described by (4.1.1), an observer type that is similar to the before described extended Luenberger observer is chosen. This results in the output observer being of the form of

$$\dot{\hat{z}} = \begin{bmatrix} cos(\hat{\theta}) & 0 \\ sin(\hat{\theta}) & 0 \\ 0 & 1 \end{bmatrix} \begin{bmatrix} v \\ \omega \end{bmatrix} + K \begin{bmatrix} y_1 - \hat{z_1} \\ y_2 - \hat{z_2} \\ y_3 - \hat{z_3} \end{bmatrix} \tag{4.1.7}$$

which is similar to the observer described in [8].

$$K = \begin{bmatrix} K_{11} & K_{12} & K_{13} \\ K_{21} & K_{22} & K_{23} \\ K_{31} & K_{32} & K_{33} \end{bmatrix} \tag{4.1.8}$$

$$E = A - KC \tag{4.1.9}$$

In (4.1.7), the matrix K is a 3×3 gain matrix. It must be chosen such that the observer error, which is given as a matrix E in (4.1.9), is Hurwitz. The observer error describes an error of observation that can be caused by the observer failing to correctly observe the system. For it to be Hurwitz, all eigenvalues must have negative real parts.

4.1.1 Eigenvalues

In order to obtain a K-matrix such that the error matrix is Hurwitz, the eigenvalues are subjected to closer inspection. The eigenvalues of the error matrix result in a diagonal matrix of the form of

$$eig(E) = \begin{bmatrix} -K_{11} & 0 & 0 \\ 0 & -K_{22} & 0 \\ 0 & 0 & -K_{33} \end{bmatrix} \tag{4.1.10}$$

As can be seen, the eigenvalues are equal to the chosen diagonal values of the gain matrix. The diagonal values thus have to be chosen accordingly, such that their real parts are positive to ensure the negative eigenvalues.

4.2 Offset observer

Since there is a constant offset present in the measurement data of θ, this offset is incorporated in the observer as a separate state to make an estimation of its magnitude. Considering this, a new state space representation of the nonlinear system must be defined.

$$\begin{aligned} \dot{z} = f(y,u,t) &= \begin{bmatrix} cos(\theta) & 0 \\ sin(\theta) & 0 \\ 0 & 1 \\ 0 & 0 \end{bmatrix} \begin{bmatrix} v \\ \omega \end{bmatrix} \\ y = h(z,t) &= \begin{bmatrix} 1 & 0 & 0 & 0 \\ 0 & 1 & 0 & 0 \\ 0 & 0 & 1 & 1 \end{bmatrix} \begin{bmatrix} z_1 \\ z_2 \\ z_3 \\ z_4 \end{bmatrix} \end{aligned} \tag{4.2.1}$$

Here, $\dot{z}$ is defined as $\begin{bmatrix} \dot{x} & \dot{y} & \dot{\theta} & \dot{\theta}_{off} \end{bmatrix}^{\mathrm{T}}$, z thus as $\begin{bmatrix} x & y & \theta & \theta_{off} \end{bmatrix}^{\mathrm{T}}$ and the measured output y is given as $\begin{bmatrix} x & y & \theta \end{bmatrix}^{\mathrm{T}}$. θ_{off} is constant, so the derivative of this constant is independent of either v or ω. The measurement θ is now comprised of the sum of itself and the offset.

Following the trend of (4.1.2) to (4.1.4), the system is linearized again to determine its observability. The state space representation including the Jacobian is now given by (4.2.2). As with the output observer, an extended Luenberger observer is chosen, which is given for the offset observer by (4.2.3), where the only main difference with the output observer is the inclusion of the additional state θ_{off}. The gain matrix K is now of the size 4×3.

$$\begin{aligned} \dot{z} &= \begin{bmatrix} 0 & 0 & -v\sin\theta & 0 \\ 0 & 0 & v\cos\theta & 0 \\ 0 & 0 & 0 & 0 \\ 0 & 0 & 0 & 0 \end{bmatrix} \begin{bmatrix} x \\ y \\ \theta \\ \theta_{off} \end{bmatrix} + \begin{bmatrix} cos(\theta) & 0 \\ sin(\theta) & 0 \\ 0 & 1 \\ 0 & 0 \end{bmatrix} \begin{bmatrix} v \\ \omega \end{bmatrix} \\ y &= \begin{bmatrix} 1 & 0 & 0 & 0 \\ 0 & 1 & 0 & 0 \\ 0 & 0 & 1 & 1 \end{bmatrix} \begin{bmatrix} x \\ y \\ \theta \\ \theta_{off} \end{bmatrix} \end{aligned} \tag{4.2.2}$$

$$\dot{\hat{z}} = \begin{bmatrix} cos(\hat{\theta}) & 0 \\ sin(\hat{\theta}) & 0 \\ 0 & 1 \\ 0 & 0 \end{bmatrix} \begin{bmatrix} v \\ \omega \end{bmatrix} + K \begin{bmatrix} y_1 - \hat{z_1} \\ y_2 - \hat{z_2} \\ y_3 - \hat{z_3} - \hat{z_4} \end{bmatrix} \tag{4.2.3}$$

4.2.1 Observability

Due to the altered matrices A and C for the offset observer, the matrix C in itself does not guarantee observability of the system anymore. Therefore, the rank of the observability matrix must be checked. Now, n is equal to 4. So, in order for the system to be observable, the rank of the observability matrix must be equal to 4 as well. Since higher order computations of CA^n all result in 3×4 zero matrices, only the observability of matrix C in combination with matrix CA has to be checked:

$$O_{reduced}(C, A) = \begin{bmatrix} 1 & 0 & 0 & 0 \\ 0 & 1 & 0 & 0 \\ 0 & 0 & 1 & 1 \\ 0 & 0 & -v \sin\theta & 0 \\ 0 & 0 & v \cos\theta & 0 \\ 0 & 0 & 0 & 0 \end{bmatrix} \tag{4.2.4}$$

From (4.2.4), it follows that the observability of the system is always guaranteed as long as the velocity v of the unicycle is not equal to zero. For more information on the proof of the observability, Appendix A can be consulted.

4.2.2 Eigenvalues

Next to the observability of the system, the eigenvalues of the error matrix also have to be re-determined to ensure that the error matrix is Hurwitz. However, in contrast with the output observer, the eigenvalues of the offset observer are not simply equal to the chosen diagonal values of the gain matrix, but are dependent on all entries of the gain matrix and the states in a complex manner. Therefore, the eigenvalues are checked manually for any chosen K-matrix during simulation.

Chapter 5

Experiments and results

This chapter contains the experiment plan for testing the behavior of the two observers, and the results of the executed experiments, which are found in Section 5.1 and 5.2 respectively. The experiment plan is used to structure the course of experimenting, and to give an overview of which experiments are conducted. The results give an overview of the stability and performance of the two designed observers.

5.1 Experiment plan

As discussed previously, the actual e-puck setup at the Dynamics and Control lab cannot be accessed due to the COVID-19 outbreak in the Netherlands. In order to still obtain truthful results for the observer, signals are generated using MATLAB that imitate the behavior of the e-puck robot in the setup. Such a signal consists of two parts: a so-called ground truth signal, GT-signal, and a measured signal, the MM-signal. The GT-signal imitates the expected behavior of the e-puck as closely as possible. The output of this signal is ideally the output the observer should also generate. The MM-signal on the other hand, imitates the output as measured by the camera in the setup. This output thus contains, for example, an applied angular offset of 0.01 rad and applied setup noise, such as camera noise for example. The latter signal with errors is used in combination with the observer. If the observer is working properly, it should be able to compensate for the applied offset and applied noise. As soon as the observer is able to do this perfectly, the output of the observer should essentially be the same as the initially generated GT-signal. It is therefore that the difference between the observer output and the GT-signal is a measure for the performance of the observer. This difference is called the 'observer error', and is described by (5.1.1), where $y_{observer}$ is the output of the observer and y_{GT} the output of the GT-signal.

$$e_{observer} = y_{observer} - y_{GT} \tag{5.1.1}$$

In order to be able to draw conclusions from the observer error, the root-mean-square value of the error and the maximum error of a trajectory are evaluated. Here, the root-mean-square value is used to ensure that negative errors and positive errors do not cancel each other out. This could lead to a lower average error and might give one wrong impressions about the observer performance.
The goal for the performance of the observer is expressed in a set of requirements, being as follows:

The observer is said to have a proper performance if

- the maximum error value for output state x is lower than $|0.01|$ meters
- the maximum error value for output state y is lower than $|0.01|$ meters
- the maximum error value for output state θ is lower than $|0.1|$ radials

With these requirements in mind, the research into the performance of the observers is split into three sections; manoeuvres, initial conditions and the applied θ_{off}.
In the section Manoeuvres, the gain matrices K are determined for both observers, using multiple signals with different kinds of trajectories. This is done to ensure that the observers perform accordingly for all kinds of trajectories. To this end, four signals are generated, namely a trajectory of a straight line, a circle, an infinity-shaped trajectory and a trajectory that resembles a sine wave. Whilst constructing the K matrices, the stability of the observers is taken into account by checking the eigenvalues of the error matrices, as explained earlier.
The section Initial Conditions evaluates the convergence of the observers to the GT-signal trajectory over time for initial conditions that do not match the initial conditions of the MM-signal. The reason for this is that, in the actual setup, the chance that the e-puck robot is placed exactly in its desired initial pose, is very small. It is likely that due to human error, the initial pose will be off in the directions x, y and θ. Therefore, small deviations are created in the initial conditions to mimic this error.
Lastly, in the section Applied θ_{off}, the observers' performances are evaluated for different values of θ_{off}. As the observer are to be used in a setup where an angular offset is often present, the largest angular offset for which the observers still perform desirable is determined.
For all research sections, the behavior of the output observer is compared to the behavior of the offset observer, to see which one performs better.

5.2 Results

5.2.1 Manoeuvres

Of all the signals used to determine the gain matrices, the MM- and GT-signals can be seen in Figures 5.2.1 to 5.2.4. As is seen in the figures, the GT-signals show neat motions, while the MM-signals show errors in x- and y-direction, as expected. Next to the MM- and GT-signals, also the so called desired behavior is shown. This is the ideal trajectory of the unicycle, where no setup noise or offsets are included at all. The main difference between the desired behavior and the ground truth, is that the ground truth shows the actual trajectory that the e-puck drives in the setup, where the desired behavior can be seen as the "pure" signal that is send to the e-puck. The differences between these two signals are caused by e-puck noise, for example, frictions on the e-puck wheels.
Firstly, the gain matrix of the output observer is determined. This gain matrix is relatively straight forward and easy to construct due to the simplicity of the previously mentioned eigenvalues of the error matrix. It is therefore that this one is determined first, to get an insight in the workings of the observer.

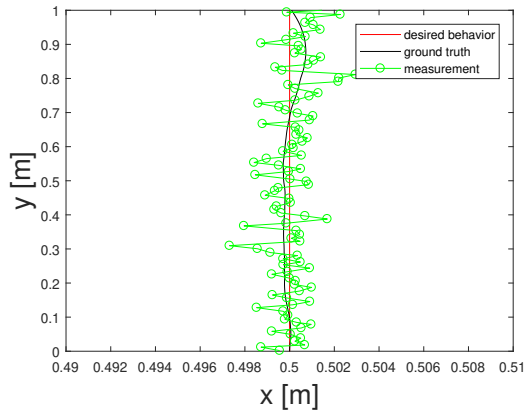

Figure 5.2.1: Line signal, generated with input states $v = 0.1\ m\ s^{-1}$ and $\omega = 0\ rad\ s^{-1}$

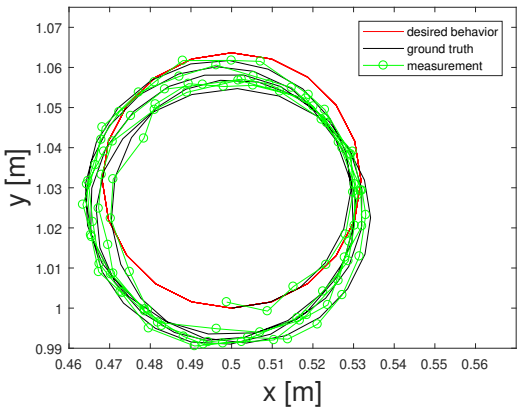

Figure 5.2.2: Circle signal, generated with input states $v = 0.1\ m\ s^{-1}$ and $\omega = \pi\ rad\ s^{-1}$

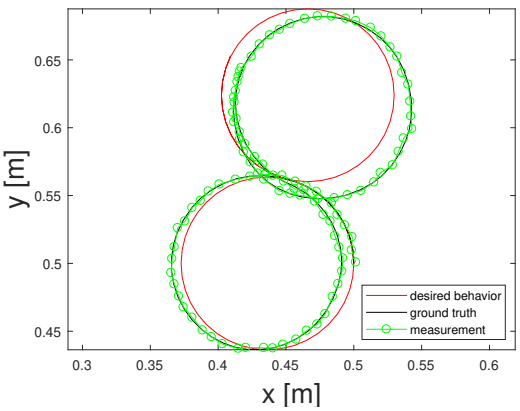

Figure 5.2.3: Infinity signal, generated with input states $v = 0.1\ m\ s^{-1}$ and $\omega = -0.5\pi\ rad\ s^{-1} \vee \omega = 0.5\pi\ rad\ s^{-1}$

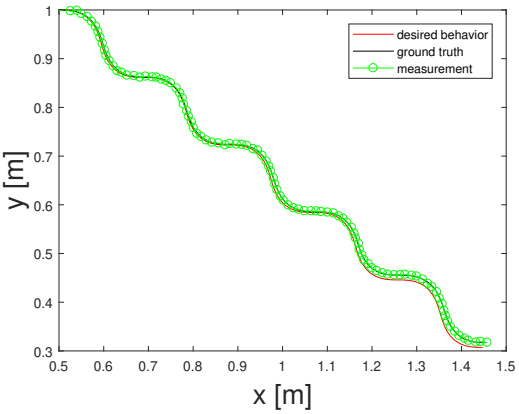

Figure 5.2.4: Sinus signal, generated with input states $v = v_{max}\ m\ s^{-1}$ and $\omega = -2\sin \pi t\ rad\ s^{-1}$

After several experiments, the K-matrix that fits best with the set requirements of the observer performance is found to be:

$$K_{output} = \begin{bmatrix} 1 & 0 & 0 \\ 0 & 1 & 0 \\ 0 & 0 & 25 \end{bmatrix} \tag{5.2.1}$$

where all the entries on the diagonal are positive, ensuring negative and real eigenvalues. The observer is thus stable for all input signals. Using this gain matrix, the output results of the observer as illustrated in Table 5.2.1 have been obtained.

Table 5.2.1: The results for the output observer for the four manoeuvres and for the given gain matrix K_{output}.

	RMS of error			Maximum error		
Signal	**x [m]**	**y [m]**	**θ [rad]**	**x [m]**	**y [m]**	**θ [rad]**
Line	0.0010	0.0022	0.0101	-0.0015	0.0053	0.0124
Circle	0.0017	0.0013	0.0126	-0.0034	0.0029	0.0146
Infinity	0.0012	0.0013	0.0102	0.0027	-0.0035	0.0262
Sinus	0.0015	0.0019	0.0109	0.0033	0.0048	0.0162

From the table, it can be concluded that the output observer meets the performance requirements, as all RMS values and maximum errors are below the allowed error of 0.01 for x and y and 0.1 for θ.

The same is done for the offset observer. Now, the stability of the observer must be checked more closely, due to the complex nature of the eigenvalues. Using the same signals as described before, the K-matrix for the offset observer is found to be:

$$K_{offset} = \begin{bmatrix} 1 & 0 & 0 \\ 0 & 1 & 0 \\ 0 & 0 & 25 \\ 0.01 & 0.01 & 1 \end{bmatrix} \tag{5.2.2}$$

Using this gain matrix, the output results of the observer as illustrated in Table 5.2.2 have been obtained.

Table 5.2.2: The results for the offset observer for the four manoeuvres and for the given gain matrix K_{offset}.

	RMS of error			Maximum error			Stability
Signal	**x [m]**	**y [m]**	**θ [rad]**	**x [m]**	**y [m]**	**θ [rad]**	**-**
Line	0.0009	0.0022	0.0099	-0.0015	-0.0053	0.0120	Stable
Circle	0.0017	0.0014	0.0256	-0.0038	0.0029	0.0365	Partially stable
Infinity	0.0012	0.0014	0.0128	0.0027	-0.0035	0.0253	Partially stable
Sinus	0.0015	0.0019	0.0104	0.0033	0.0048	0.0155	Unstable

From Table 5.2.2, it can be concluded that the performance requirements for the observer are met. The observer, however, is not stable for all signals. This can be seen when the eigenvalues are evaluated as a function of θ. Because the state matrix A is dependent on θ, the eigenvalues differ for different inputs of ω. This is illustrated in Figure 5.2.5 for θ ranging from -2π to 2π. The second eigenvalue of the error matrix fluctuates between positive and negative real values, and thus introduces instability for certain values of θ. Take, for example, the line signal. Because this signal uses an input value of approximately $\omega = 0\ rad\, s^{-1}$, see GT-signal, it thus ensures constant stability. However, signals with fluctuating ω input values might thus not be stable all the time. The eigenvalues as function of θ, used to determine the stability of the other manoeuvres, can be found in Appendix B, Figures B.1.1 to B.1.3.

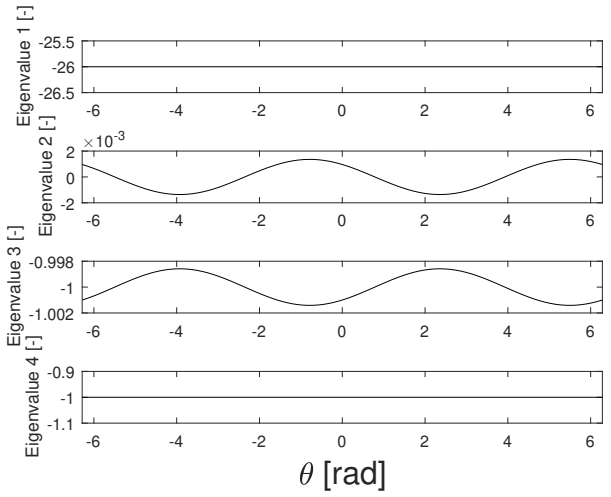

Figure 5.2.5: The four eigenvalues of the error matrix the offset observer as function of θ in the domain $[-2\pi, 2\pi]$

5.2.2 Initial conditions

By changing the initial conditions of the observer, so they do not match the initial conditions of the MM-signal anymore, the convergence of the observer trajectory to the GT-signal is evaluated. This is done by determining the settling time t_0 at which the observer error is equal to the requirement for the first time. The smaller the value of t_0, the better the observer performs. As initial conditions, for x, y and θ, twice the allowed maximum error is added to the initial condition as follows from the MM-signal; $\begin{bmatrix} \mathrm{IC}_x + 0.02 & \mathrm{IC}_y + 0.02 & \mathrm{IC}_\theta + 0.2 \end{bmatrix}^{\mathrm{T}}$ for the output observer and $\begin{bmatrix} \mathrm{IC}_x + 0.02 & \mathrm{IC}_y + 0.02 & \mathrm{IC}_\theta + 0.2 & 0 \end{bmatrix}^{\mathrm{T}}$ for the offset observer respectively.

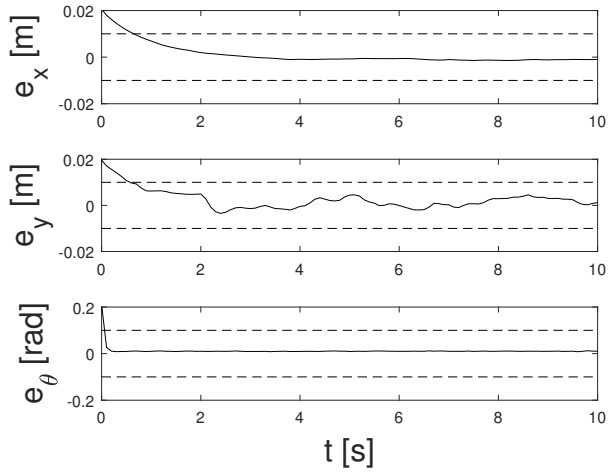

Figure 5.2.6: The error of the output observer with applied initial conditions offsets over time for the Line signal. The dashed lines correspond with the required error values for the different output states. t_0 is here defined as the settling time which corresponds with the time at which the error, for the first time, is smaller than the requirement.

In Figure 5.2.6, an example is given for the convergence of the error. The dashed lines in the plots represent the requirements of the error. t_0 is thus found where the observer error and the dashed line intersect. Similar figures for the error as function of time for the other signals and for the offset observer can be found in Appendix B.

Table 5.2.3: The results for the settling time t_0 for the altered initial conditions

	t_0 **output observer**			t_0 **offset observer**		
Signal	**x [s]**	**y [s]**	θ **[s]**	**x [s]**	**y [s]**	θ **[s]**
Line	0.7	0.6	0.1	0.7	0.6	0.1
Circle	0.5	1.0	0.1	0.5	1.0	0.1
Infinity	0.7	0.6	0.1	0.7	0.6	0.1
Sinus	0.9	0.8	0.1	1.0	0.9	0.1

As can be seen in Table 5.2.3, both observers have the same settling times t_0 for the observer error of the states x, y and θ over the same trajectory for most signals. However, this is not the case for the Sinus signal. Here, the output observer shows slightly better performance than the offset observer. But, since the sampling frequency of the signals is equal to 10 Hz, this could be caused by rounding due to too large time intervals. To investigate whether there truly is a difference between the settling time for the observers for the Sinus signal, it is advised to use a larger sampling frequency on the generated signals.

5.2.3 Applied θ_{off}

The used offset so far on the MM-signals used to be $0.01\,rad$. Now, a θ_{off} of $0.05\,rad$, $0.1\,rad$ and $0.5\,rad$ are applied to the signals. Here, only the signals Line and Infinity are tested, because these two signals are representative for multiple manoeuvres, as the signals include straight and curved trajectories in positive and negative $\dot{\theta}$-directions.

Table 5.2.4: The results for the output observer with varying applied θ_{off}, Line signal

	RMS of error			**Maximum error**		
Applied θ_{off} **[rad]**	**x [m]**	**y [m]**	θ **[rad]**	**x [m]**	**y [m]**	θ **[rad]**
0.05	0.0046	0.0029	0.0500	-0.0053	-0.0067	0.0518
0.1	0.0094	0.0020	0.1001	-0.0104	0.0055	0.1021
0.5	0.0437	0.0128	0.4999	-0.0477	0.0183	0.5018

Table 5.2.5: The results for the offset observer with varying applied θ_{off}, Line signal

	RMS of error			**Maximum error**		
Applied θ_{off} **[rad]**	**x [m]**	**y [m]**	θ **[rad]**	**x [m]**	**y [m]**	θ **[rad]**
0.05	0.0046	0.0029	0.0495	-0.0053	-0.0067	0.0517
0.1	0.0094	0.0020	0.0997	-0.0104	-0.0055	0.1017
0.5	0.0435	0.0126	0.4971	-0.0473	0.0183	0.5009

For both observers, the results are in principle the same for the varying applied θ_{off}, as shown by Tables 5.2.4 and 5.2.5. Neither of the observers shows a significant better performance.

When looking more closely at the RMS values of the error and the maximum error of the different signals, it becomes apparent that for an applied θ_{off} of 0.1 rad, both observers still just about meet their requirements. For the applied θ_{off} of 0.5 rad, however, the requirements are no longer met and both observers are not deemed operational. The results for this applied offset are sometimes up to five times as large as allowed.

Table 5.2.6: The results for the output observer with varying applied θ_{off}, Infinity signal

	RMS of error			**Maximum error**		
Applied θ_{off} [rad]	**x [m]**	**y [m]**	**θ [rad]**	**x [m]**	**y [m]**	**θ [rad]**
0.05	0.0020	0.0024	0.0499	-0.0043	0.0054	0.0685
0.1	0.0044	0.0046	0.1000	-0.0087	-0.0080	0.1179
0.5	0.0215	0.0194	0.4999	-0.0381	0.0316	0.5178

Table 5.2.7: The results for the offset observer with varying applied θ_{off}, Infinity signal

	RMS of error			**Maximum error**		
Applied θ_{off} [rad]	**x [m]**	**y [m]**	**θ [rad]**	**x [m]**	**y [m]**	**θ [rad]**
0.05	0.0021	0.0025	0.0523	-0.0047	0.0056	0.0671
0.1	0.0046	0.0046	0.1026	-0.0091	-0.0081	0.1165
0.5	0.0216	0.0195	0.5021	-0.0384	0.0316	0.5159

Also for the Infinity signal, hardly any differences between the results for the output observer and the offset observer can be found for the same applied θ_{off}. Tables 5.2.6 and 5.2.7 do not show either one of the observers to outperform the other. Again, the observers both perform desirable for an applied offset of 0.05 rad, showing no apparent problems with meeting the requirements. At an applied θ_{off} of 0.1 rad, the observers just about meet the requirements, where mainly the RMS error and maximum error of θ are slightly too high to meet the requirements. The applied θ_{off} of 0.5 rad proves to be too much for the observers to handle properly, as is also seen at the Line signal.

The main difference between the Line signal and the Infinity signal is found when looking at the RMS values of the error for the state x. As can be seen, the RMS values for the Line signal are about twice as large as for the Infinity signal. This can be explained by the fact that the observer trajectory of the Infinity signal crosses the trajectory of the GT-signal, thus resulting in a lower RMS value. As for the Line signal, the trajectories do not cross. This can be seen in Figures 5.2.7 and 5.2.8, where this is illustrated for an applied θ_{off} of 0.1 rad. It is therefore, in this case, better to compare the maximum error values of the state x.

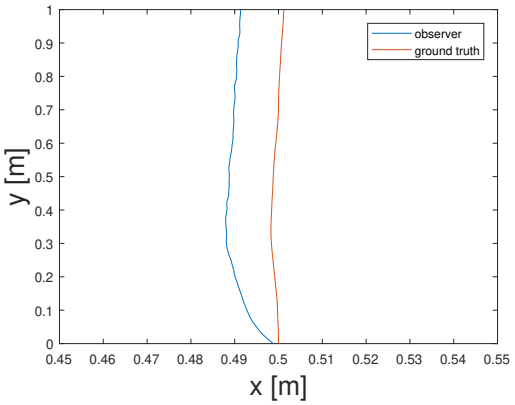

Figure 5.2.7: The trajectory of the output observer versus the trajectory of the GT-signal for the Line signal, as a function of the position in the xy-plane. With an applied offset of 0.1 *rad*.

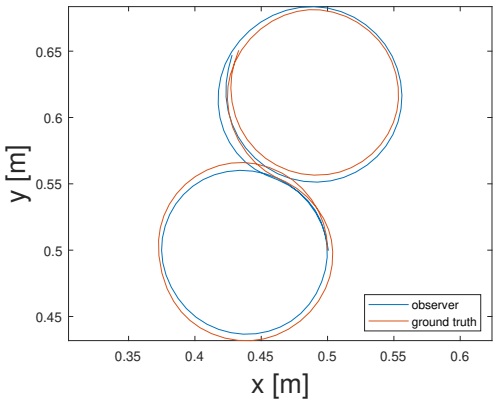

Figure 5.2.8: The trajectory of the output observer versus the trajectory of the GT-signal for the Infinity signal, as a function of the position in the xy-plane. With an applied offset of 0.1 *rad*.

5.3 Comparison of observers

As became apparent from the results, with the chosen gain matrices, both observers meet the requirements with respect to the performance for all manoeuvres. Furthermore, there is no distinct difference between the performance results of the output observer versus the offset observer with respect to the convergence for divergent initial conditions. Also, both observers perform similarly for the same applied offset values on the same type of signals. For both the Line signal and the Infinity signal, an maximum possible applicable offset of 0.1 *rad* is found. Since the Line and the Infinity signal are deemed to be representative for multiple kinds of manoeuvres, it can be assumed that the found maximum possible applied offset is the same for other trajectories.
However, one of the main drawbacks of the offset observer is that, where the output observer is always stable for each input signal, the offset observer is not. Within a spectrum of $[-2\pi, 2\pi]$, the real part of the second eigenvalue of this observer shifts multiple times from a negative value to a positive one. This renders the observer for three out of the four tested manoeuvres (partially) unstable. This is an important feature that must be taken into account upon choosing to use this observer in real life setups.

Chapter 6

Conclusion and recommendations

6.1 Conclusion

In this project, two observers are developed for unicycle type mobile robots that both estimate the pose of the robot, and of which one also estimates the angular offset. Both observers are based on a kinematic model of the e-puck robot. This kinematic model treats the e-puck robot as a unicycle type mobile robot, which uses inputs velocity v and angular velocity ω, to define its pose in a 2D-plane. As output, the states x, y and θ are chosen. From the model, a clear angular offset became apparent compared to measured results of the setup.
Based on the kinematic model, an observer type that is similar to an extended Luenberger observer is chosen. Of this observer, two versions are developed. One version that is based on the system outputs, and one that includes an additional state θ_{off} to estimate the found angular offset. Both observers give similar results for different kinds of manoeuvres of the e-puck trajectory, for the convergence to the original trajectory for divergent initial conditions and for varying applied θ_{off}. The maximum applied θ_{off} the observers can deal with is found to be 0.1 rad. However, as the observer that uses the additional state θ_{off} is not stable for all input values of state ω due to the dependency of state matrix A on state θ, this observer must be treated with care if applied in real life setups.

6.2 Recommendations

One of the main issues for this project was the closure of the Dynamics and Control Department at the university campus, where the physical e-puck setup is located. The MATLAB generated signals are assumed to closely relate to actual setup results, and are therefore deemed representative enough to obtain reliable results. However, as estimations of setup noise are made in the process, it is recommended to verify the found results in this project using the actual setup if possible.

As became apparent, the offset observer is not always stable for all input values of ω. As a stable observer is normally desired, two suggestions are given on how to improve the observer.
One of the options is to use a time dependent K-matrix. By doing so, the gain matrix can be made dependent of the state θ. Since the second eigenvalue is varying over θ, these variations could ideally be cancelled out this way. A suggestion would be to use gain matrix entries

that are of the form of $\sin\theta$ or $\cos\theta$. During this project, little time has been invested in this option, but the results seemed promising.
An other way to put the results of the offset observer to good use, is to only use this observer to estimate the θ_{off} of an e-puck robot. This can be done by tuning the gain matrix very precisely for a specific signal of which the stability is ensured at all times. The offset observer creates a very accurate approximation of the angular offset, which can then be used in combination with the output observer. Since the output observer does not show stability issues, the found θ_{off} can than be used to correct for the state θ in the output observer, thus creating a reliable observer.

Bibliography

[1] École Polytechnique Fédérale de Lausanne. (2010). e-puck official website. Retrieved from http://www.e-puck.org/index.php?option=com_content&view=article&id=6&Itemid=3

[2] Trifa, V.M., Cianci, C.M., Guinard, D. (2008). Dynamic Control of a Robotic Swarm using a Service-Oriented Architecture. Proceedings of International Symposium on Artificial Life and Robotics, Beppu, Japan.

[3] Slusny, S., Neruda, R., Vidnerova, P. (2008). Learning Algorithms for Small Mobile Robots: Case Study on Maze Exploration. In Proceedings of the Conference on Theory and Practice of Information Technologies.

[4] Van Den Broek, T. H. A., Van De Wouw, N., Nijmeijer, H. (2009). Formation control of unicycle mobile robots: A virtual structure approach. Proceedings of the IEEE Conference on Decision and Control, 8328–8333.

[5] Luenberger, D. G. (1966). Observers for Multivariable Systems. IEEE Transactions on Automatic Control, 11(2), 190–197.

[6] Zeitz, M. (1987). The extended Luenberger observer for nonlinear systems. Systems and Control Letters, 9(2), 149–156.

[7] Busawon, K. K., Saif, M. (1999). A state observer for nonlinear systems. IEEE Transactions on Automatic Control, 44(11), 2098–2103.

[8] Sundarapandian, V. (2010). Nonlinear observer design for Nonlinear Pendulum Systems. International Journal of Advanced Research in Computer Science, 1(03), 348–353.

[9] Thau, F.E. (1973). Observing the states of nonlinear dynamical systems. International J. Control, 18, 471-479.

[10] Krener, A. J., Isidori, A. (1983). Linearization by output injection and nonlinear observers. Systems and Control Letters, 3, 47–52.

[11] Spurgeon, S. K. (2008). Sliding mode observers: A survey. International Journal of Systems Science, 39(8), 751–764.

[12] Hongwei, W., Heping, W. (2015). A Comparison Study of Advanced Tracking Differentiator Design Techniques. Procedia Engineering, 99, 1005–1013.

[13] Han, J. (1995). A class of extended state observers for uncertain systems. Control and Decision, 10(1), 85-88. (In Chinese)

[14] Gao, Z. (2003). Scaling and Parameterization Based Controller Tuning. Proceedings of the American Control Conference, 6, 4989- 4996.

[15] Van De Wouw, N. (2020). Dynamics and Control of Robotic Systems: Mobile Robotics [Powerpoint slides]. Retrieved from `https://canvas.tue.nl/courses/10035/files`

Appendix A

Appendix Chapter 4

In Appendix A, all additional information for Chapter 4 is given. This includes the proof of the observability of the system with the additional angular offset state θ_{off}

A.1 Proof of observability of system with additional state θ_{off}

As discussed in Chapter 4, the observability of the system can be checked with the reduced observability matrix:

$$O_{reduced}(C,A) = \begin{bmatrix} 1 & 0 & 0 & 0 \\ 0 & 1 & 0 & 0 \\ 0 & 0 & 1 & 1 \\ 0 & 0 & -v\sin\theta & 0 \\ 0 & 0 & v\cos\theta & 0 \\ 0 & 0 & 0 & 0 \end{bmatrix} \tag{A.1.1}$$

In order to obtain the maximal number of linearly independent ranks, either one of the following statements must be valid:

1. $1 + nv\sin\theta = 0$ (1), while at the same time $v\cos\theta + mv\sin\theta = 0$ (2)
2. $1 + nv\cos\theta = 0$ (3), while at the same time $v\sin\theta + mv\cos\theta = 0$ (4)

Where n and m can be any number required, since in the same row where the sine and cosine terms are situated, all other entries are 0. The above mentioned statements are valid if and only if:

1. (1) $\theta \neq 0 + k\pi$ and $v \neq 0$, while at the same time (2) $\theta \neq 0 + k\pi$ or $\theta = 0.5\pi + k\pi$
2. (3) $\theta \neq 0.5\pi + k\pi$ and $v \neq 0$, while at the same time (4) $\theta \neq 0.5\pi + k\pi$ or $\theta = 0 + k\pi$

Where k can be any integer. Therefore, since the validations contradict each other, the nonlinear system with additional state θ_{off} is always observable as long as $v \neq 0$.

Appendix B

Appendix Chapter 5

In Appendix B, all additional information for Chapter 5 is given. This includes figures for the stability of the eigenvalues of the offset observer and figures for the convergence of the output states to the GT-signal for altered initial conditions. All these figures support results that are given in Chapter 5.

B.1 Stability of eigenvalues offset observer for different manoeuvres

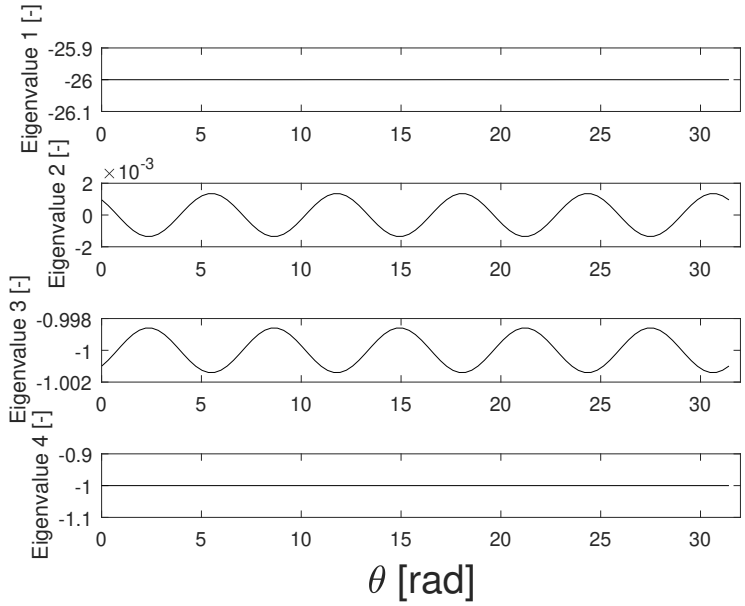

Figure B.1.1: The four eigenvalues of the error matrix of the Circle signal as function of θ, rendering the observer partially stable

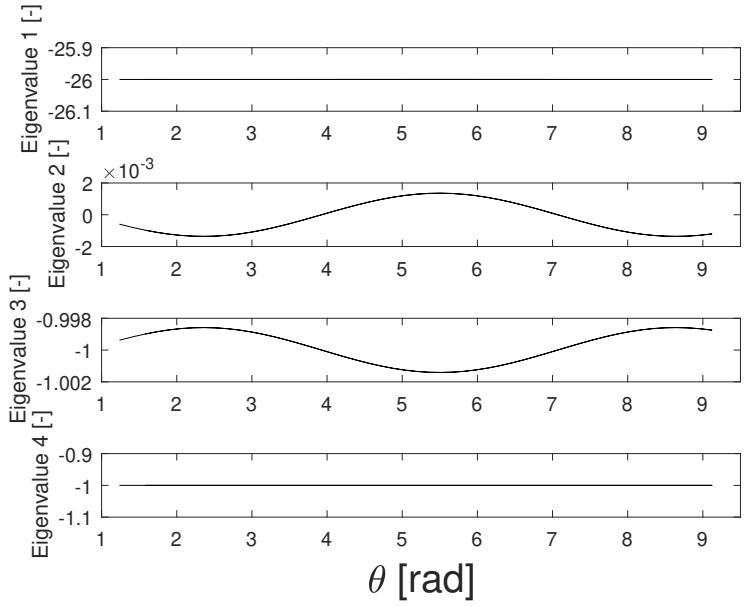

Figure B.1.2: The four eigenvalues of the error matrix of the Infinity signal as function of θ, rendering the observer partially stable

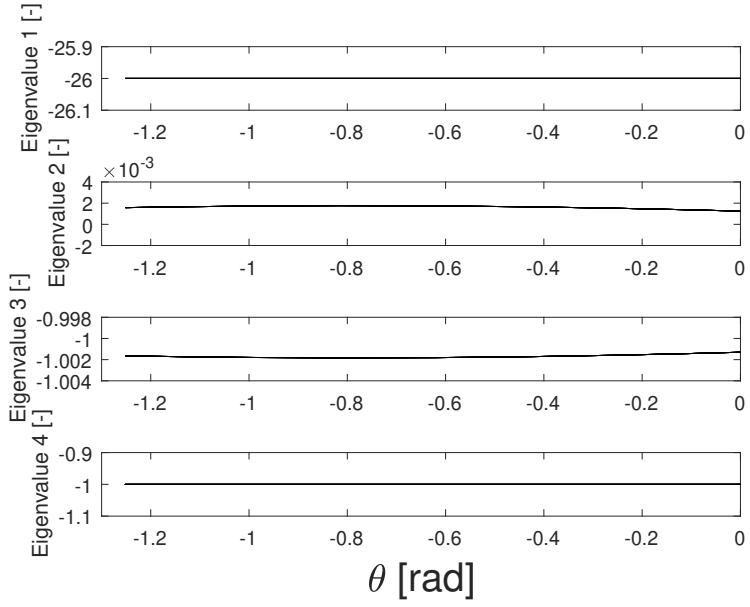

Figure B.1.3: The four eigenvalues of the error matrix of the Sinus signal as function of θ, rendering the observer unstable

B.2 Convergence of the output states for altered initial conditions

B.2.1 Output observer

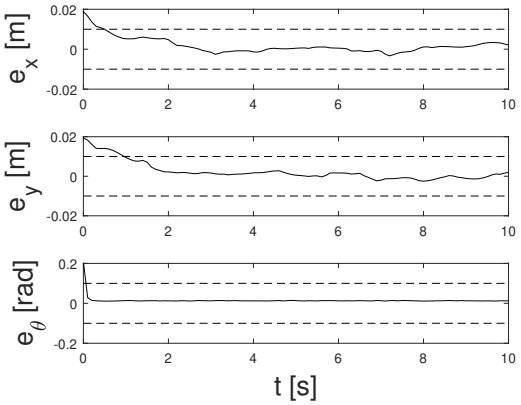

Figure B.2.1: The error of the output observer with applied initial offsets over time for the Circle signal.

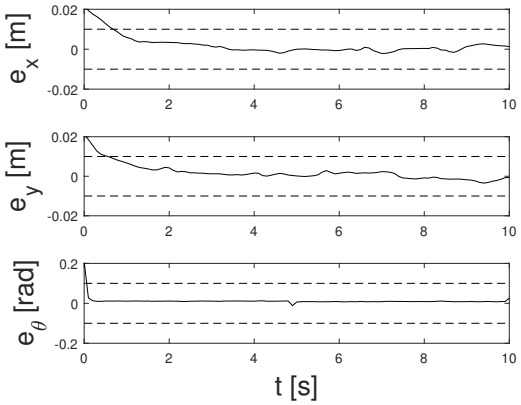

Figure B.2.2: The error of the output observer with applied initial offsets over time for the Infinity signal.

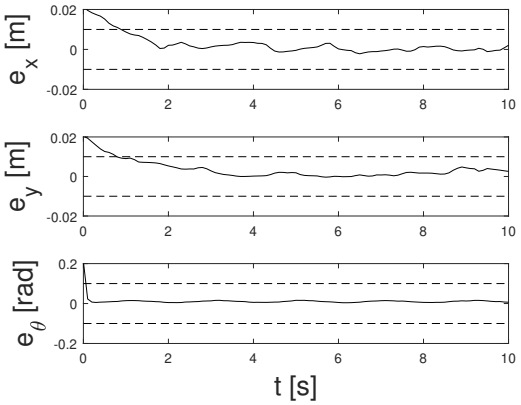

Figure B.2.3: The error of the output observer with applied initial conditions offsets over time for the Sinus signal.

B.2.2 Offset observer

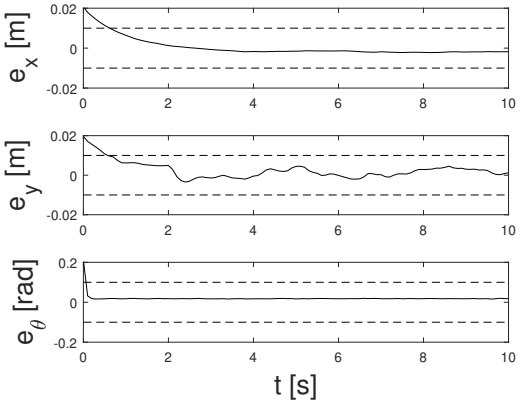

Figure B.2.4: The error of the offset observer with applied initial conditions offsets over time for the Line signal.

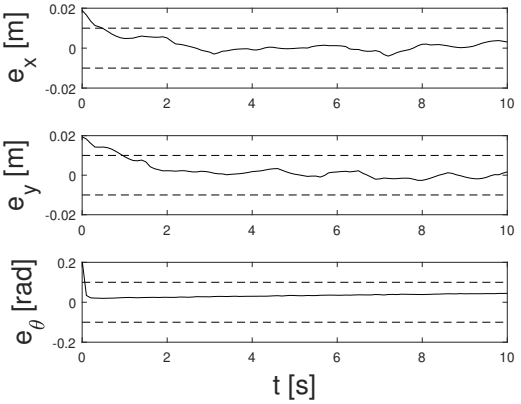

Figure B.2.5: The error of the offset observer with applied initial conditions offsets over time for the Circle signal.

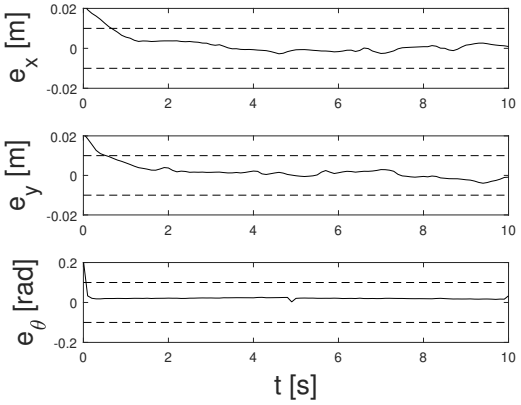

Figure B.2.6: The error of the offset observer with applied initial conditions offsets over time for the Infinity signal.

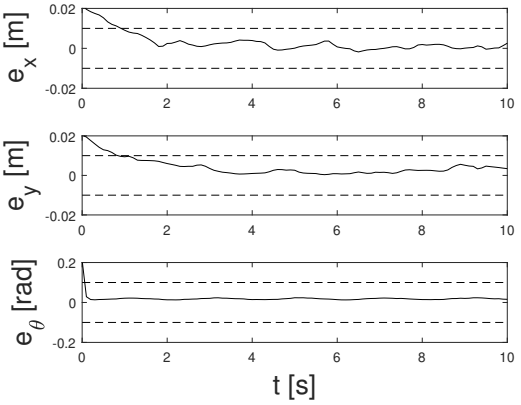

Figure B.2.7: The error of the offset observer with applied initial conditions offsets over time for the Sinus signal.